Mechanism of the Non-Kasha Fluorescence in Pyrene

Sourav Majumdar, Robin Grotjahn* Ahmadreza Rajabi, Bibo Feng†,
Luke Nambi Mohanam‡, Gabriel S. Phun§, Nicolas Lutfi,
Mohammad Khan,¶ Dmitrij Rappoport, and Filipp Furche‖

Department of Chemistry, 1102 Natural Sciences II,
University of California Irvine, Irvine CA, 92697-2025, USA

December 30, 2024

Abstract

The high-energy shoulder in the gas-phase fluorescence emission spectrum of pyrene is a well-known example of non-Kasha emission. We comparatively assess two approaches, vibronic perturbation theory and nonadiabatic dynamics, in their ability to predict and explain the gas-phase fluorescence spectrum of pyrene. While both methods qualitatively capture the non-Kasha emission, they differ in their computational requirements, accuracy, and physical interpretation. Vibronic perturbation theory and nonadiabatic dynamics are complementary and can be combined in a two-step approach to non-Kasha fluorescence.

Keywords: Non-Kasha fluorescence, vibronic coupling, nonadiabatic dynamics, conical intersections, time-dependent density functional theory ∎

*Present address: Department of Chemistry and Biochemistry, Santa Clara University, Santa Clara, CA 95053, USA

†Present address: Tufts University School of Medicine, MA 02111, USA

‡Present address: Department of Chemistry, Lehigh University, PA 18015, USA

§Present address: Department of Materials Science and Engineering, University of California, Riverside, CA 92521, USA

¶Present address: The University of Texas at Dallas, TX 75080, USA

‖Corresponding author. Email: filipp.furche@uci.edu

Nonadiabatic Dynamics

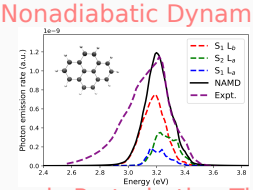

Vibronic Perturbation Theory

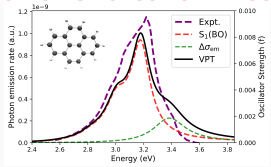

Two approaches, vibronic perturbation theory and nonadiabatic dynamics, are comparatively assessed in their ability to predict and explain the gas-phase fluorescence spectrum of pyrene.

I Introduction

The steady-state fluorescence of many stable (singlet) organic molecules is adequately described by the empirical Kasha's rule, which posits that their emission should only proceed from their S_1 states.[45] The conventional rationale for Kasha's rule is that the internal conversion (IC) from $S_n \rightarrow S_1$ ($n > 1$) is typically very fast compared to the S_1 fluorescence lifetime. Steady-state non-Kasha fluorescence can arise through several distinct mechanisms[13,21,42,43,78,80], posing a difficult challenge for electronic structure and quantum dynamics methods; it has important applications, e. g., the design of dually fluorescent dyes for biological imaging or artificial photosynthesis.[12,21,42] Pyrene and some of its derivatives, such as benzopyrene, obey Kasha's rule in solution[9], the gas-phase fluorescence is more complex, with an additional high-energy emission ($> 3.4\,\mathrm{eV}$)[4,16,34,42,80]. The high-energy shoulder is enhanced in a collision-free environment and is diminished when the pressure of the inert gas in the reaction mixture is increased.[3,15,16]

Here we consider the non-Kasha fluorescence of pyrene in the gas phase within equilibrium response theory and semiclassical nonadiabatic molecular dynamics (NAMD). Equilibrium response theory, specifically vibronic perturbation theory, provided the first successful rationale for pyrene's non-Kasha emission in the 1970s[2,25,47,55]. It is suitable for steady-state processes and longer timescales, and inexpensive enough to allow for quantum nuclear treatment, typically within the rigid rotor-harmonic oscillator (RRHO) model. However, this approach requires *a priori* knowledge of the critical points (equilibrium structures, conical intersections) of the relevant potential energy surfaces (PESs). Moreover, electronic structure methods capable of providing potential energy surface and derivative couplings accurate enough to test vibronic perturbation theory for molecules of the size of pyrene have become available only in the recent past.

Semiclassical NAMD simulations[72,77] using high-level electronic structure methods to compute energies, gradients, and nonadiabatic couplings on-the-fly were pioneered by Lischka and co-workers[6,48] and have been increasingly used to study ultrafast processes far from equilibrium. While NAMD simulations require little prior knowledge and can be considered "computational experiments", longer timescales in the ps to ns regime are computationally

demanding for larger polyatomic molecules. Recently, Isborn and co-workers[86] have shown that NAMD simulations may fail to reproduce vibronic effects which can be attributed to the fact that the nuclei are treated semiclassically.[86] Vibronic effects in the emission spectrum of pyrene have been studied extensively[19,27,33,35,37,50] and thus offer a good test case for a comparative assessment of equilibrium response theory vs. NAMD simulations.

A recent study by Barbatti and co-workers[13] used NAMD simulations with the second-order Algebraic Diagrammatic Construction (ADC(2))[67,76] to study the non-Kasha fluorescence of pyrene in the gas phase. The couplings between the electronic states were calculated using the local diabatization algorithm[62] and the spectrum was calculated by averaging over a large number of time steps. The non-Kasha fluorescence was found to result from a dynamic equilibrium between the S_1 and S_2 states, leading to a significant contribution from the bright S_2 state in the emission spectrum. The strong nonadiabatic coupling between the S_1 and S_2 states suggests the presence of an accessible conical intersection (CI) between S_1 and S_2 adiabatic PESs. Maeda and co-workers[39] investigated CIs between the ground (S_0) and the S_1 states of pyrene and similar polycyclic aromatic hydrocarbons and found a correlation between the energy barrier to the CI and the fluorescence quantum yield. Robb and co-workers[75] explored the CI between the first two excited states of the pyrene radical cation to understand its role in the diffuse interstellar bands. The existence of such a CI and its role in the S_2 to S_1 ultrafast relaxation was studied by de Vivie-Riedle and co-authors[65] using both semiclassical and quantum dynamics simulations.

A key question addressed in this work is whether the non-Kasha fluorescence of pyrene can be understood in terms of static vibronic mixing or whether it is a fundamentally dynamic effect resulting from an equilibrium between the S_1 and S_2 states. We simulate the emission spectrum of pyrene by vibronic perturbation theory using parameters obtained from time-dependent density functional theory (TDDFT) calculations. We also perform fewest-switches surface hopping (FSSH) NAMD simulations[77] at the same level of electronic structure theory.[60,66,72,74,81] In Section II, we describe the theoretical methods used in this study. In Section III, we present the results of our vibronic perturbation theory and NAMD simulations. These two approaches are compared in Section IV, and we present conclusions in Section V.

II Methods

A Vibronic Perturbation Theory

Conventional vibronic perturbation theory uses fixed-position (crude adiabatic) Born-Oppenheimer[10,38,44] (BO) wavefunctions as the basis for the perturbation expansion and treats the dependence of the electronic wavefunction on the nuclear coordinates as a perturbation.[2,25] The zero-order terms in the perturbation expansion are the Franck–Condon (FC) contributions, while the first-order terms are the Herzberg–Teller (HT) terms. In this paper, we start from adiabatic BO electronic states within the RRHO (rigid rotor harmonic oscillator) approximation as our zero-order states in the spirit of Ref. 54. The BO RRHO spectra including FC factors and Dushinsky rotation are efficiently computed using the generating function approach[70,73]. We then consider HT coupling and first-order nonadiabatic couplings (FONAC), $\mathbf{F}_{nm} = \langle \Phi_n | \frac{\partial}{\partial R} \Phi_m \rangle$ with respect to nuclear coordinates R between adiabatic states Φ_n and Φ_m as a perturbation. Within the dipole approximation, the isotropically averaged first-order photon emission rate from a fixed initial state i is given by[54]

$$\sigma_{\mathrm{em}}(\omega) = \frac{4\omega^3}{3c^3} \sum_f |\boldsymbol{\mu}_{if}|^2 G(\omega - \omega_{if}). \tag{1}$$

The transition dipole moment

$$\boldsymbol{\mu}_{if} = \langle \Psi_i | \hat{\boldsymbol{\mu}} | \Psi_f \rangle \tag{2}$$

is defined in terms of eigenstates of the full molecular Hamiltonian, Ψ_i and Ψ_f, whose energy difference is ω_{if}. ω denotes the emission energy, $G(\omega)$ is a normalized lineshape function, and c denotes the speed of light. Atomic (Hartree) units are used throughout; in these units, energies and (angular) frequencies are identical, since $\hbar = 1$. Eq. (1) can be extended to finite temperature by considering an ensemble initial state[54].

We expand the transition dipole moment $\boldsymbol{\mu}_{if}$ around its BO-RRHO value $\boldsymbol{\mu}_{if}^{(0,0)}$ as

$$\boldsymbol{\mu}_{if} = \boldsymbol{\mu}_{if}^{(0,0)} + \boldsymbol{\mu}_{if}^{(0,1)} + \boldsymbol{\mu}_{if}^{(1,0)} + \boldsymbol{\mu}_{if}^{(1,1)} + \text{higher-order terms}. \tag{3}$$

$\boldsymbol{\mu}_{if}^{(0,1)}$ accounts for the first-order HT correction to $\boldsymbol{\mu}_{if}^{(0,0)}$, whereas $\boldsymbol{\mu}_{if}^{(1,0)}$ corrects for FONAC; $\boldsymbol{\mu}_{if}^{(1,1)}$ is a second-order correction taking both effects into account. Computing the HT corrections using finite differences for the S_1 state of pyrene is numerically nontrivial and

requires careful convergence studies, see Supporting Information (SI). FONAC corrections were evaluated using analytical first-order nonadiabatic couplings[56,60,68]; the only intermediate state giving rise to significant nonadiabatic couplings at the S_1 minimum structure is S_2. The thus obtained HT corrections to the transition dipole moment were found to be more than two orders of magnitude smaller in magnitude than the FONAC corrections. Moreover, $\boldsymbol{\mu}_{if}^{(1,0)}$ and $\boldsymbol{\mu}_{if}^{(0,0)}$ are orthogonal by symmetry. The lowest-order correction to the BO-RRHO emission spectrum of pyrene is thus

$$\Delta\sigma_{\mathrm{em}}(\omega) = \frac{4\omega^3}{3c^3} \sum_f |\boldsymbol{\mu}_{if}^{(0,1)}|^2 G(\omega - \omega_{if}). \tag{4}$$

The lineshape was assumed to be Gaussian with an empirically chosen root mean square (RMS) width of 0.058 eV. The theoretical spectrum was red-shifted by 0.45 eV to facilitate comparison to the experimental spectrum[4].

B NAMD Simulations

Electronic Structure Multi-state NAMD simulations[60,72] were performed using the fewest-switches surface hopping methods using density functional theory (DFT) with the PBE0 functional[61] along with D3-dispersion corrections.[36] Excitation energies[7,28,30,40], excited-state gradients[29,31,32], ground-to-excited state FONAC vectors[68] were computed using the Tamm–Dancoff approximation (TDA)[20,23,40,69]. The TDA approximation to TDDFT is known to describe the L_a and L_b states of polycylic aromatic hydrocarbons more accurately than full TDFFT and also provides reliable absorption and fluorescence spectrum band shapes[14,41,83]. The FONAC vectors between excited states were computed from quadratic response TDDFT in the wavefunction approximation[56,58–60]. def2-SVPD basis sets were used for carbon[64,84], and def2-SVP basis sets were used for hydrogen[84]. The initial conditions for the NAMD simulations were sampled from a 10 ps long ground-state molecular dynamics simulation after an equilibration period of 0.5 ps. The ground-state calculations used def2-SVP basis sets throughout. The molecular dynamics trajectories were propagated using the leapfrog Verlet algorithm[79] with the time step of 20 a. u. The same time step size was used for the propagation of NAMD trajectories. A microcanonical ensemble of trajectories was initiated from both S_1 and S_2 states to replicate the excited state dynamics of pyrene in a collision-free

regime. All calculations were performed with the TURBOMOLE program suite, Version V7.5[1,26]. The NAMD simulations were performed using TURBOMOLE modules such as EGRAD[31] and FROG[24,71].

Trajectory Analysis and Spectroscopic Observables The electronic properties of a trajectory at any given time are determined by a single Born–Oppenheimer electronic state, referred to as the active state. The instantaneous population $p_m(t)$ of an electronic state S_m ($m = 0$ corresponds to the ground state) was computed from the proportion of trajectories with active state m at time t. The lifetime of the S_2 state was estimated by fitting the decay of the state population to an exponential function. The 95% confidence intervals for the state populations were calculated using bootstrap resampling with 10 000 bootstrap samples.[51,52,60]

The fluorescence emission spectrum was computed by averaging the instantaneous emission spectrum over the trajectory ensemble[18] after an initial equilibration period of 0.5 ps. Instantaneous emission spectra were evaluated according to Eq. (1), using the excitation energies and electronic BO transition dipole moments of the active state. A Gaussian linewidth function with an empirical RMS linewidth of 0.01 eV was used. The theoretical spectrum was red-shifted by 0.45 eV to facilitate comparison to the experimental spectrum[4].

Conical Intersection and Intersection Space The minimum energy CI (MECI) between the S_1 and S_2 adiabatic states was obtained using the CI optimization algorithm of Maeda and co-workers[49] implemented in the ORCA program package[53]. The energy gap, $E_2 - E_1$, at the MECI was found to be less than 1 meV, which is on the same order of magnitude as the convergence criterion used for the excited state calculations. The intersection space vectors, the nonadiabatic coupling ($\boldsymbol{h}$) and the difference gradient ($\boldsymbol{g}$) were computed at the S_1/S_2 MECI geometry. The $\boldsymbol{g}$ and $\boldsymbol{h}$ vectors were used to generate a 12×12 2D grid of pyrene structures centered on the MECI structure by nuclear displacement in Cartesian space. At each grid point, a single-point TDDFT calculation was performed. The minimum energy structures of the S_m ($m = 0, 1, 2$) were optimized. All calculations were performed using the TDA approximation to TDDFT with the PBE0 functional, def2-SVPD basis set and

D3-dispersion corrections. The projections of these critical points on the two-dimensional intersection space were located by minimizing the root mean square distances (RMSD) between optimized global minimum energy structures and the ones from the generated PES. The RMSD between two structures were computed using the quaternion algorithm[82] using the open-source rmsd program[46].

III Results

A Excited States of Pyrene

The two lowest-lying adiabatic electronic excited states (S_1 and S_2) of pyrene are involved in the photoexcitation and photoemission process in the UV-visible region. These two adiabatic electronic states have either bright L_a or dark L_b diabatic state characters with the transition dipole moment aligned along the short and long axis of the molecule respectively according to Platt's notation[27,63]. We observed that the L_a state mainly results from a highest occupied molecular orbital (HOMO) to lowest unoccupied molecular orbital (LUMO) transition while the L_b state mainly results from a near equal mixture HOMO to LUMO + 1 and HOMO-1 to LUMO transitions in agreement with previous computational studies[57]. At the ground state minimum or the FC point, S_1 has dark L_b diabatic state character and S_2 has bright L_a diabatic state character. The two excited states were optimized starting from the FC point. The S_1 and S_2 states were found to have the same L_b and L_a diabatic state characters at the ground state, S_1 and S_2 minimum energy structures and at the MECI between the S_1 and S_2 states. The molecular orbitals involved in the $S_0 \rightarrow S_1$ and $S_0 \rightarrow S_2$ transitions at the critical point structures have been included in Section I of the SI. The comparison between vertical excitation energies and absorption spectra at the TDA/PBE0 level with experimental results has been included in Section I of the SI as well.

B NAMD Trajectory Analysis

An ensemble of $n_{\text{traj}} = 40$ trajectories was propagated for $T = 2000$ time steps (corresponding to 1 ps) after initial excitation to the S_2 state. Starting on the S_2 state, pyrene quickly

populated the S_1 state, while the S_2 population decayed exponentially with a lifetime of 40 fs (Table 1). This is comparable to the experimental lifetime of 85 fs computed using transient absorption spectroscopy[11]. After the $S_2 \rightarrow S_1$ relaxation, the further transfer to the S_0 state was too slow to produce reliable statistics. The experimental lifetime of the S_1 state of pyrene measured in degassed solvent was found to be 354 ns[17]. However, two separate regions of the S_1 PES could be identified in the simulations based on the comparison of the oscillator strengths f_1 and f_2 of the S_1 and S_2 states, respectively. The structures with $f_1 < f_2$ were considered as having L_b (dark) character[63], while the structures with $f_1 \geq f_2$ were assigned to the L_a (bright) character. The transition dipole moment vectors of the structures with L_a character were found to be parallel to the short axis of the molecule, while the vectors of the structures with L_b character were parallel to the long axis of the molecule. The structures from the trajectories evolving on the S_2 state were found to have L_a character.

The S_1 state with dark L_b character predominated in the trajectory ensemble (94.83%, Table 1). The average occupation of the S_2 state was small (2.35%), reflecting the fast relaxation to the S_1 state. The trajectories also occupied the S_1 state with L_a character (0.91%). The remaining occupation can be attributed to a single trajectory which switched to the ground state after 600 fs (Figure 2, Table 1).

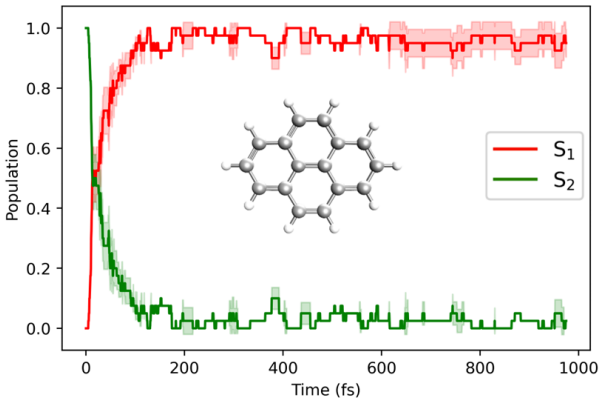

Figure 1: The population of the S_1 and S_2 states of pyrene as a function of time. The shaded regions indicate the 95% confidence intervals obtained by bootstrap resampling.

State m	$\bar{p}_m$[%]	$\bar{E}_m$, eV	$\bar{f}_m$
S_2	2.35	3.73	0.281
S_1 (L_a)	0.91	3.68	0.356
S_1 (L_b)	94.83	3.62	0.010
S_0	1.90	0.0	0.0

Table 1: State occupations, $\bar{p}_m$, average energies, $\bar{E}_m$, and oscillator strengths, $\bar{f}_m$, (length gauge) of the S_m, $m = 1, 2$, states of pyrene from NAMD simulations with $n_{\text{traj}} = 40$ trajectories and simulation time $T = 1\,\text{ps}$ after an equilibration period of 0.5 ps.

C NAMD Fluorescence Spectrum

The spectrum exhibits two separate bands. The low-energy band ($< 3.4\,\text{eV}$) is higher in intensity and is attributed to emission from the S_1 state with L_b character. The high-energy band ($> 3.4\,\text{eV}$) contains emission from S_1 and S_2 states with L_a character (Figure 2). However, the thus obtained spectra depend on the lineshape function: Smaller linewidths lead to a distinct shoulder in the high-energy region but fail to reproduce the low-energy tail of the spectrum, whereas the high-energy shoulder is obscured when using larger linewidths that more adequately reproduce the width of the experimental spectrum. Although, NAMD accounts for anharmonicity to a certain degree the computed spectrum lacks the vibrational structure present in the experimental spectrum which is reproduced by the VPT S_1 (BO) spectrum (Figure 3).

D Vibronic Perturbation Theory

The simulated fluorescence spectrum of pyrene using the vibronic perturbation theory expression, 4, is shown in Figure 3. The lower-energy band is due to FC transition from the relaxed S_1 state with L_b character. The adiabatic excitation energy of the S_1 state is $E_1^{\text{ad}} = 3.72\,\text{eV}$, and the norm of electronic transition dipole moment is $|\boldsymbol{\mu}_{01,\text{el}}| = 0.104\,\text{a.u.}$ The high-energy shoulder arises from the first-order correction $\Delta\sigma_{\text{em}}$ due to FONAC of the S_1 and S_2 states. The S_1 and S_2 states are coupled by a single "promoting" mode which is nearly parallel to the FONAC vector (Figure 4).

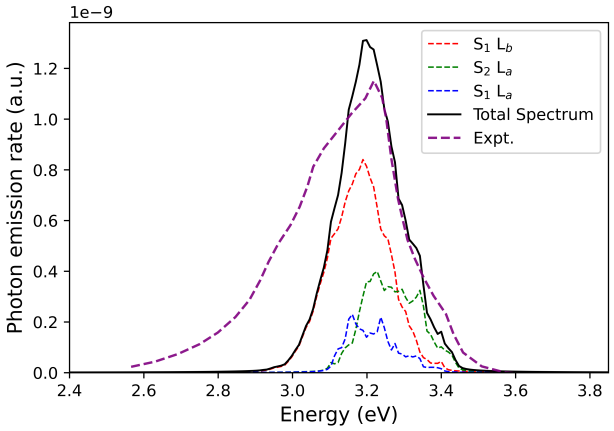

(a)

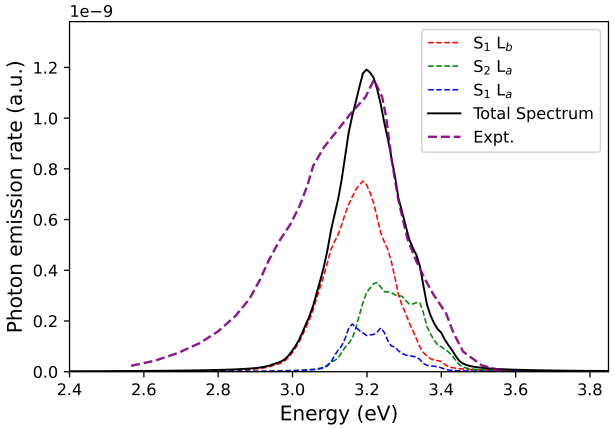

(b)

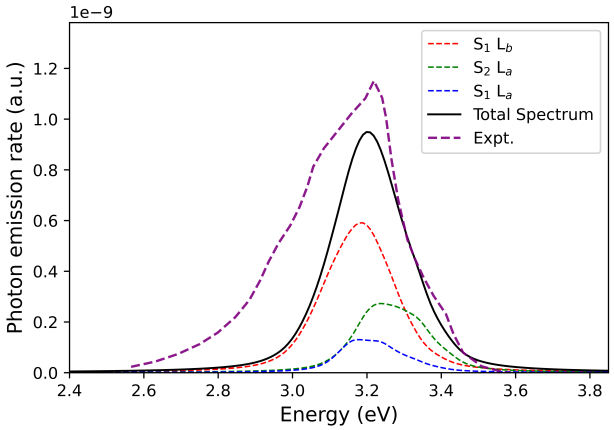

(c)

Figure 2: Fluorescence emission spectrum of pyrene simulated by NAMD in comparison with experiment[4]. The relative experimental intensities were scaled to match the vibronic perturbation theory intensities, see Fig. 3. Lorentzian linewidths of (a) 0.005 eV, (b) 0.01 eV, and (c) 0.03 eV were used. All computed spectra were red-shifted by 0.45 eV to facilitate comparison with experiment.

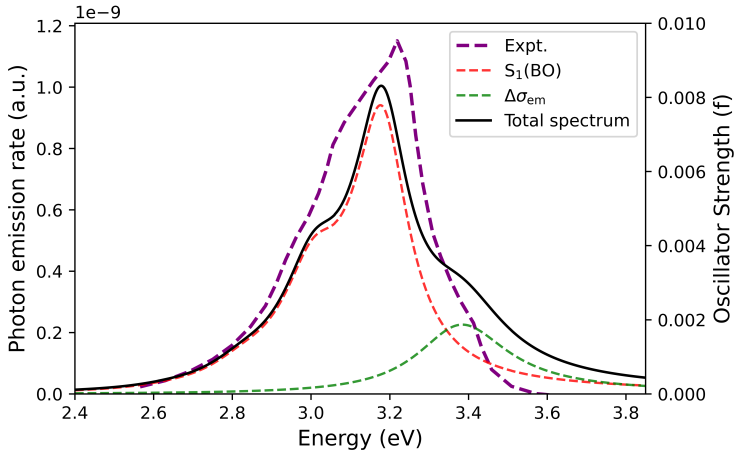

Figure 3: Fluorescence emission spectrum of pyrene obtained from vibronic perturbation theory in comparison with experiment[4]. The relative experimental intensities were scaled to match the computed intensities. The zero-order BO spectrum was determined by FC simulations using the generating function approach[70], whereas the FONAC correction $\Delta\sigma_{em}$ was simulated using a Lorentzian centered at the adiabatic S_2 excitation energy with a linewidth of 0.15 eV. All computed spectra were red-shifted by 0.45 eV to facilitate comparison with experiment.

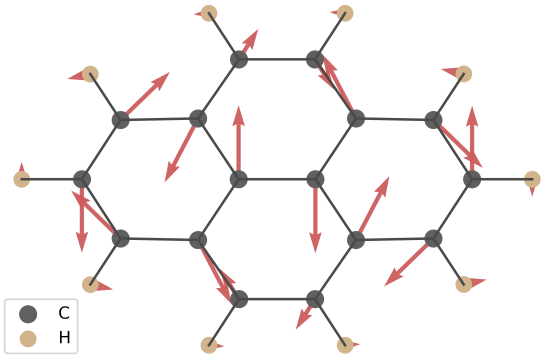

Figure 4: The promoting mode, i.e., the S_1 normal model with largest overlap with the S_1-S_2 FONAC vector. Displacements are indicated by arrows. All displacements are in the molecular plane.

The S_2 emission energy is determined by computing the difference in energy between the initial and final vibronic levels of the S_2 and S_0 states, which is equal to the adiabatic excitation energy of the S_2 state is $E_2^{\mathrm{ad}} = 3.86\,\mathrm{eV}$. The corresponding electronic transition dipole moment norm is $|\boldsymbol{\mu}_{02,\mathrm{el}}| = 1.778\,\mathrm{a.u.}$ The magnitude of the Herzberg–Teller contribution terms $|\boldsymbol{\mu}_{if}^{(0,1)}| = 0.0004$ and $|\boldsymbol{\mu}_{if}^{(1,1)}| = 0.0002$ were found to be small in comparison to the FONAC terms $|\boldsymbol{\mu}_{if}^{(1,0)}| = 0.05$, due to the weak dependence of the the electronic transition dipole moments of the $S_0 \rightarrow S_1$ and $S_0 \rightarrow S_2$ transitions on the nuclear coordinates. The S_1 (BO) contribution of VPT spectrum includes the vibrational structure of the spectrum computed using the harmonic approximation (FC spectrum). Due to the limitations of the current implementation of VPT, the $\Delta\sigma_{\mathrm{em}}$ contribution to the spectrum does not include the computation of the vibrational structure and instead the S_2 adiabatic excitation energy is used as an approximation to the emission energy. The full set of simulation results is presented in the Section III of the SI.

E Intersection Space

The energetic and emission parameters of the S_1 and S_2 states of pyrene in the intersection space are shown in Figure 5. The changes in the oscillator strengths illustrate that the character of the S_1 state switches from dark L_b to bright L_a and vice versa for the S_2 state. Due to the rigidity of the pyrene molecule, the minimum-energy structures of the excited S_1 and S_2 states, as well as the S_0 ground state (FC point), exhibit a high degree of structural similarity. The MECI structure lies 0.12 eV higher than the S_1 energy minimum and 0.01 eV higher than the S_2 minimum. Moreover, the FC point of the S_1 PES is only 0.08 eV above the MECI, see Table 2. The energy differences are approximately preserved in the intersection space, which indicates the the two-dimensional representation captures the essential features of the full multidimensional PESs in the vicinity of the CI.

IV Discussion

The interpretation of the non-Kasha behavior of pyrene differ depending on the theoretical framework used. NAMD simulations of pyrene indicate that the high-energy shoulder in

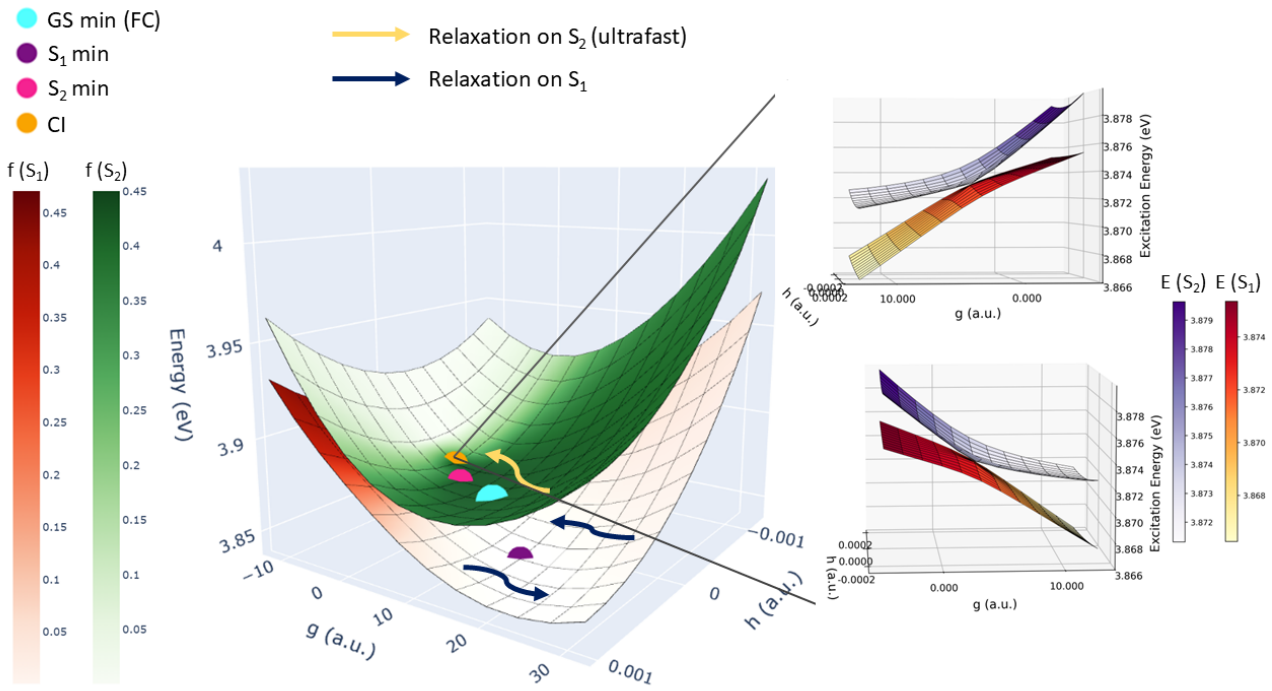

Figure 5: Energies of the S_1 and S_2 excited states of pyrene in the intersection space around the S_1/S_2 minimum energy conical intersection (MECI). The projections of the S_0 energy minimum (FC point), S_1, S_2 energy minima energy structures, and the MECI point are shown. Insert: Enlarged view of the vicinity of the MECI, with energies the S_1 and S_2 states shown on a color scale.

Structure	E_m [eV]	E'_m [eV]
FC	3.956	3.876
S_1 min.	3.752	3.845
S_2 min.	3.861	3.870
MECI	3.873	3.873

Table 2: Electronic energies, E_m, (eV) of the S_m, $m = 1, 2$ energy minima, the minimum energy conical intersection (MECI) point, and the FC point of pyrene and energies E'_m of the critical point projections on the intersection space. All energies are given relative to the ground-state S_0 minimum energy. No vibrational energy corrections were applied.

Figure 2 can be explained in terms of a reverse internal conversion $S_2 \rightarrow S_1$, as previously suggested by Barbatti and co-workers[13], but also as a result of the change in state character of the S_1 state between L_b (dark) and L_a (bright). As Table 1 shows, the average oscillator strength of the region of the S_1 PES with L_a character is comparable to that of the S_2 state, which results in a non-negligible contribution to the high-energy emission, see Figure 2. NAMD is suitable for simulating the non-Kasha behavior involving emission from multiple electronic states as it requires the description of several excited state transitions. Pure BO excited state MD is less suitable for this purpose as such simulations are restricted to the PES of a single electronic state and offers minor computational advantage.

Equilibrium response theory is generally far less computationally demanding than NAMD simulations. Approaches such as the FC and the Franck–Condon Herzberg–Teller (FCHT), usually only include emission occurs from the lowest-lying electronic excited state.[5,22,73] The FCHT method additionally takes into account the variation of the transition moment with respect to nuclear displacements. However, the FC and FCHT do not adequately describe the vibronic effects in emission spectrum of pyrene.[27,33] The present results show that vibronic perturbation theory provides an accurate description of the fluorescence spectrum of pyrene, including the high-energy shoulder, if (i) the HT couplings are accurately computed, (ii) the nonadiabatic coupling between the S_1 and S_2 states is included as an additional perturbation. The inference that FONAC terms dominate HT terms is only possible if the HT couplings are computed carefully. Implementations based on finite differences may provide erroneous results due to large default displacement size as demonstrated by the results of the numerical calculations in Section III of the SI. The correction to the transition dipole moment due to FONAC, $\boldsymbol{\mu}_{if}^{(1,0)}$, is found to be 0.05 a.u. in magnitude, only slightly less than the zero-order BO S_1 transition dipole moment. The HT corrections are several orders of magnitude smaller.

V Conclusions

Both NAMD and vibronic perturbation theory qualitatively capture the non-Kasha fluorescence of gas-phase pyrene. Strong nonadiabatic coupling between the S_1 and S_2 states is the

origin of the non-Kasha fluorescence emission, even though the pictures emerging from both approaches appear very different: The vibronic calculations show clear evidence of "intensity stealing" by nonadiabatic mixing of the S_1 and S_2 BO states: Even at the S_1 equilibrium structure, the nonadiabatic coupling is strong enough to allow for virtual excitations into low-lying excited vibrational levels of S_2 which emit to the ground state. In the NAMD simulations, on the other hand, the CI between S_1 and S_2 is crucial for the non-Kasha emission, because it enables population transfer between the two BO surfaces. While the picture emerging from the NAMD simulations is intuitively appealing, it does not imply that the non-Kasha fluorescence of pyrene is a fundamentally "dynamic" effect. Rather, our vibronic perturbation calculations suggest that the S_2 population observed in the semiclassical trajectory simulations mimics the vibronic mixing between the "static" nuclear wavefunctions of the two BO states.

Our results confirm semiclassical NAMD simulations as a valuable tool for mechanistic discovery, because they can be run with relatively little user input and will capture a wide variety of different mechanisms, at least if the timescale is short enough. Moreover, NAMD simulations are fundamentally capable of describing transient processes far from equilibrium. A major downside of NAMD simulations is their relatively high computational cost; also, the resulting spectra typically lack structure and may show incorrect intensities due to the use of semiclassical nuclei. The use of empirical lineshape functions is particularly problematic for pyrene, because the relatively small high-energy shoulder disappears from the NAMD spectrum for larger linewidths. Moreover, while including thermal effects in NAMD simulations is straightforward, it can be difficult to distinguish them from nuclear quantum effects, which are treated on the same footing within FSSH. While more sophisticated treatments of nuclear quantum effects[8,85] may address these issues, they are even more resource-intensive than semiclassical NAMD.

Equilibrium response theory is much more confined in scope, but rather inexpensive compared to NAMD simulations when using electronic structure methods of similar complexity. In particular, the results of this work suggest that extending existing efficient approaches for the calculation of FC spectra[70,73] to incorporate nonadiabatic effects may be worthwhile, particularly for the simulation of high-resolution steady-state spectra. Since NAMD sim-

ulations and vibronic perturbation theory are complementary, they can be synergistically combined in a two-step approach: NAMD simulations can be used initially to "scout" the potential energy surfaces and qualitatively identify key mechanisms and stationary points of interest, followed by more refined vibronic calculations yielding accurate spectral intensities.

Acknowledgments

A. R. acknowledges support from an Eddleman Quantum Institute fellowship. R. G. acknowledges support via a Walter-Benjamin postdoctoral fellowship funded by the Deutsche Forschungsgemeinschaft (DFG, German Research Foundation) – 501114520. This material is based upon work supported by the U.S. Department of Energy, Office of Basic Energy Sciences, under Award Number DE-SC0025405. This work utilized the infrastructure for high-performance and high-throughput computing, research data storage and analysis, and scientific software tool integration built, operated, and updated by the Research Cyberinfrastructure Center (RCIC) at the University of California, Irvine (UCI). S. M. acknowledges insightful discussions with Zaira Barrera on the non-Kasha fluorescence mechanism.

Notes

Conflict of Interest

The authors declare the following competing financial interest(s): Principal investigator Filipp Furche has an equity interest in TURBOMOLE GmbH. The terms of this arrangement have been reviewed and approved by the University of California, Irvine, in accordance with its conflict of interest policies.

Author Contribution Statements

Sourav Majumdar: Conceptualization (equal), Methodology (lead), Software (lead), Validation (lead), Formal analysis (lead), Investigation (lead), Data Curation (equal), Writing - Original Draft (lead), Writing - Review & Editing (equal), Visualization (lead), Supervision

(supporting)

Robin Grotjahn: Conceptualization (supporting), Methodology (supporting), Software (supporting), Validation (supporting), Formal analysis (supporting), Investigation (supporting), Data Curation (supporting), Writing - Original Draft (equal), Writing - Review & Editing (equal), Visualization (supporting), Supervision (equal), Funding acquisition (supporting)

Ahmadreza Rajabi: Methodology (supporting), Software (supporting), Formal analysis (supporting), Investigation (supporting), Data Curation (supporting), Writing - Original Draft (supporting), Writing - Review & Editing (equal), Visualization (supporting), Funding acquisition (supporting).

Mohammad Khan: Software (supporting), Formal analysis (supporting), Investigation (supporting), Data Curation (supporting)

Gabriel S. Phun: Software (supporting), Investigation (supporting), Writing - Review & Editing (supporting), Supervision (supporting),

Luke Nambi Mohanam: Conceptualization (supporting), Methodology (equal), Software (supporting), Validation (equal), Writing - Review & Editing (supporting),

Noah Bibo Feng: Methodology (supporting), Software (supporting), Validation (equal), Writing - Review & Editing (supporting),

Nicolas Lutfi: Methodology (supporting), Formal analysis (supporting), Investigation (supporting), Writing - Original Draft (supporting), Writing - Review & Editing (supporting),

Dmitrij Rappoport: Conceptualization (supporting), Methodology (equal), Formal analysis (supporting), Investigation (supporting), Writing - Original Draft (supporting), Writing - Review & Editing (equal), Visualization (supporting), Supervision (equal), Funding acquisition (supporting).

Filipp Furche: Conceptualization (lead), Methodology (equal), Software (supporting), Validation (equal), Formal analysis (supporting), Investigation (supporting), Resources (lead), Data Curation (lead), Writing - Original Draft (supporting), Writing - Review & Editing (equal), Visualization (supporting), Supervision (lead), Funding acquisition (lead).

References

1. TURBOMOLE V7.5 2020, a development of University of Karlsruhe and Forschungszentrum Karlsruhe GmbH, 1989-2007, TURBOMOLE GmbH, since 2007; available from `https://www.turbomole.org`.

2. T. Azumi and K. Matsuzaki. What does the term "vibronic coupling" mean? *Photochem. Photobiol.*, 25(3):315–326, 1977. doi: 10.1111/j.1751-1097.1977.tb06918.x.

3. H. Baba and M. Aoi. Vapor-phase fluorescence spectra from the second excited singlet state of pyrene and its derivatives. *J. Mol. Spectrosc.*, 46(2):214–222, 1973. doi: 10.1016/0022-2852(73)90037-4.

4. H. Baba, A. Nakajima, M. Aoi, and K. Chihara. Fluorescence from the second excited singlet state and radiationless processes in pyrene vapor. *J. Chem. Phys.*, 55(5):2433–2438, 1971. doi: 10.1063/1.1676429.

5. A. Baiardi, J. Bloino, and V. Barone. General time dependent approach to vibronic spectroscopy including Franck–Condon, Herzberg–Teller, and Duschinsky effects. *J. Chem. Theory Comput.*, 9(9):4097–4115, 2013. doi: 10.1021/ct400450k.

6. M. Barbatti, J. Paier, and H. Lischka. Photochemistry of ethylene: A multireference configuration interaction investigation of the excited-state energy surfaces. *J. Chem. Phys.*, 121(23):11614–11624, 2004. doi: 10.1063/1.1807378.

7. R. Bauernschmitt and R. Ahlrichs. Treatment of electronic excitations within the adiabatic approximation of time dependent density functional theory. *Chem. Phys. Lett.*, 256(4):454–464, 1996. doi: 10.1016/0009-2614(96)00440-X.

8. M. Ben-Nun and T. J. Martínez. Ab initio quantum molecular dynamics. In I. Prigogine and S. A. Rice, editors, *Advances in Chemical Physics*, volume 121, pages 439–512. Wiley, New York, 2002. doi: 10.1002/0471264318.ch7.

9. J. B. Birks. *Organic Molecular Photophysics*, volume 1. Wiley, New York, 1973.

10. M. Born and R. Oppenheimer. Zur Quantentheorie der Molekeln. *Ann. Phys.*, 389(20): 457–484, 1927. doi: 10.1002/andp.19273892002.

11. R. Borrego-Varillas, L. Ganzer, G. Cerullo, and C. Manzoni. Ultraviolet transient absorption spectrometer with sub-20-fs time resolution. *Appl. Sci.*, 8(6):1–18, 2018. doi: 10.3390/app8060989.

12. G. Brancato, G. Signore, P. Neyroz, D. Polli, G. Cerullo, G. Abbandonato, L. Nucara, V. Barone, F. Beltram, and R. Bizzarri. Dual fluorescence through Kasha's rule breaking:An unconventional photomechanism for intracellular probe design. *J. Phys. Chem. B*, 119(20):6144–6154, 2015. doi: 10.1021/acs.jpcb.5b01119.

13. G. Braun, I. Borges Jr, A. J. Aquino, H. Lischka, F. Plasser, S. A. Do Monte, E. Ventura, S. Mukherjee, and M. Barbatti. Non-Kasha fluorescence of pyrene emerges from a dynamic equilibrium between excited states. *J. Chem. Phys.*, 157(15):154305, 2022. doi: 10.1063/5.0113908.

14. A. Chantzis, A. D. Laurent, C. Adamo, and D. Jacquemin. Is the Tamm-Dancoff approximation reliable for the calculation of absorption and fluorescence band shapes? *J. Chem. Theory Comput.*, 9(10):4517–4525, 2013. doi: 10.1021/ct400597f.

15. K. Chihara and H. Baba. Effects of foreign gases on dual fluorescences of pyrene vapor. *Bull. Chem. Soc. Jpn.*, 48(11):3093–3100, 1975. doi: 10.1246/bcsj.48.3093.

16. K. Chihara and H. Baba. Quenching of dual fluorescences of pyrene vapor by high-pressure oxygen or nitric oxide. *Chem. Phys.*, 25(2):299–306, 1977. doi: 10.1016/0301-0104(77)87083-3.

17. A. G. Crawford, A. D. Dwyer, Z. Liu, A. Steffen, A. Beeby, L.-O. Palsson, D. J. Tozer, and T. B. Marder. Experimental and theoretical studies of the photophysical properties of 2-and 2,7-functionalized pyrene derivatives. *J. Am. Chem. Soc.*, 133(34):13349–13362, 2011.

18. R. Crespo-Otero and M. Barbatti. Spectrum simulation and decomposition with nuclear

ensemble: formal derivation and application to benzene, furan and 2-phenylfuran. *Theo. Chem. Acc.*, 131:1237, 2012. doi: 10.1007/s00214-012-1237-4.

19. K. Cunningham, W. Siebrand, D. F. Williams, and G. Orlandi. Vibronic intensity borrowing. Deuterium effect and emission-absorption asymmetry of the $S_1 \leftarrow S_0$ transition in pyrene. *Chem. Phys. Lett.*, 20(6):496–500, 1973. doi: 10.1016/0009-2614(73)80483-x.

20. S. M. Dancoff. Non-adiabatic meson theory of nuclear forces. *Phys. Rev.*, 78(4):382–385, 1950. doi: 10.1103/PhysRev.78.382.

21. A. P. Demchenko, V. I. Tomin, and P.-T. Chou. Breaking the Kasha rule for more efficient photochemistry. *Chem. Rev.*, 117(21):13353–13381, 2017. doi: 10.1021/acs.chemrev.7b00110.

22. M. Dierksen and S. Grimme. Density functional calculations of the vibronic structure of electronic absorption spectra. *J. Chem. Phys.*, 120(8):3544–3554, 2004. doi: 10.1063/1.1642595.

23. A. Dreuw and M. Head-Gordon. Single-reference ab initio methods for the calculation of excited states of large molecules. *Chemical reviews*, 105(11):4009–4037, 2005.

24. S. D. Elliott, R. Ahlrichs, O. Hampe, and M. M. Kappes. Auto-ionised products from the reaction of sodium clusters with dioxygen: Theory and experiment. *Phys. Chem. Chem. Phys.*, 2(15):3415–3424, 2000. doi: 10.1039/B003706K.

25. G. Fischer. *Vibronic Coupling*. Academic Press, London, 1984. ISBN 9780122572401.

26. Y. J. Franzke, C. Holzer, J. H. Andersen, T. Begušić, F. Bruder, S. Coriani, F. Della Sala, E. Fabiano, D. A. Fedotov, S. Fürst, S. Gillhuber, R. Grotjahn, M. Kaupp, M. Kehry, M. Krstić, F. Mack, S. Majumdar, B. D. Nguyen, S. M. Parker, F. Pauly, A. Pausch, E. Perlt, G. S. Phun, A. Rajabi, D. Rappoport, B. Samal, T. Schrader, M. Sharma, E. Tapavicza, R. S. Treß, V. Voora, A. Wodyński, J. M. Yu, B. Zerulla, F. Furche, C. Hättig, M. Sierka, D. P. Tew, and F. Weigend. Turbomole: Today and tomorrow. *J. Chem. Theory Comput.*, 19(20):6859–6890, 10 2023. doi: 10.1021/acs.jctc.3c00347.

27. A. Y. Freidzon, R. Valiev, and A. Berezhnoy. Ab initio simulation of pyrene spectra in water matrices. *RSC Adv.*, 4(79):42054–42065, 2014. doi: 10.1039/C4RA05574H.

28. F. Furche. Molecular tests of the random phase approximation to the exchange-correlation energy functional. *Phys. Rev. B*, 64(19):195120, 2001. doi: 10.1103/PhysRevB.64.195120.

29. F. Furche. On the density matrix based approach to time-dependent density functional response theory. *J. Chem. Phys.*, 114(14):5982–5992, 2001. doi: 10.1063/1.1353585.

30. F. Furche. Developing the random phase approximation into a practical post-Kohn–Sham correlation model. *J. Chem. Phys.*, 129(11):114105, 2008. doi: 10.1063/1.2977789.

31. F. Furche and R. Ahlrichs. Adiabatic time-dependent density functional methods for excited state properties. *J. Chem. Phys.*, 117(16):7433–7447, 2002. doi: 10.1063/1.1508368.

32. F. Furche and R. Ahlrichs. Erratum: "Time-dependent density functional methods for excited state properties" [J. Chem. Phys. 117, 7433 (2002)]. *J. Chem. Phys.*, 121(24): 12772–12773, 2004. doi: 10.1063/1.1824903.

33. K. P. Geigle, J. Wolf, and G. Hohlneicher. Franck-Condon/Herzberg-Teller interferences in the ^{1}lb transitions of pyrene and chrysene. *J. Photochem. Photobiol. A*, 105(2-3):183–187, 1997. doi: 10.1016/S1010-6030(96)04607-2.

34. P. Geldof, R. Rettschnick, and G. Hoytink. Fluorescence from the second excited singlets of pyrene and 3,4-benzpyrene. *Chem. Phys. Lett.*, 4(2):59–61, 1969. doi: 10.1016/0009-2614(69)85066-9.

35. P. A. Geldof, R. P. H. Rettschnick, and G. J. Hoytink. Vibronic coupling and radiative transitions. *Chem. Phys. Lett.*, 10(5):549–558, 1971. doi: 10.1016/0009-2614(71)87035-5.

36. S. Grimme, J. Antony, S. Ehrlich, and H. Krieg. A consistent and accurate ab initio parametrization of density functional dispersion correction (DFT-D) for the 94 elements H-Pu. *J. Chem. Phys.*, 132(15):154104, 2010. doi: 10.1063/1.3382344.

37. K. Gustav and M. Storch. Vibronisches Spektralverhalten von Molekülen: XX. Theoretische Untersuchung der $S_2 \leftarrow S_0$ Absorption des Pyrens im Rahmen der Herzberg–Teller-Näherung erster Ordnung. *Monatsh. Chem.*, 123(1-2):59–62, 1992. doi: 10.1007/bf01045297.

38. G. A. Hagedorn and A. Joye. Mathematical analysis of Born-Oppenheimer approximations. In F. Gesztesy, P. Deift, C. Galvez, P. Perry, and W. Schlag, editors, *Spectral Theory and Mathematical Physics*, pages 203–226. American Mathematical Society, Providence RI, 2007. doi: 10.1090/pspum/076.1/2310204.

39. Y. Harabuchi, T. Taketsugu, and S. Maeda. Exploration of minimum energy conical intersection structures of small polycyclic aromatic hydrocarbons: toward an understanding of the size dependence of fluorescence quantum yields. *Phys. Chem. Chem. Phys.*, 17(35):22561–22565, 2015. doi: 10.1039/C5CP02103K.

40. S. Hirata and M. Head-Gordon. Time-dependent density functional theory within the Tamm–Dancoff approximation. *Chem. Phys. Lett.*, 314(3-4):291–299, 1999. doi: 10.1016/S0009-2614(99)01149-5.

41. S. Hirata, M. Head-Gordon, J. Szczepanski, and M. Vala. Time-dependent density functional study of the electronic excited states of polycyclic aromatic hydrocarbon radical ions. *J. Phys. Chem. A*, 107(24):4940–4951, 2003. doi: 10.1021/jp0301913.

42. T. Itoh. Fluorescence and phosphorescence from higher excited states of organic molecules. *Chem. Rev.*, 112(8):4541–4568, 2012. doi: 10.1021/cr200166m.

43. T. Itoh. Intramolecular mechanisms for the occurrence of fluorescence from upper excited states of aromatic molecules and linear polyenes. In C. D. Geddes, editor, *Reviews in Fluorescence 2015*, chapter 9, pages 213–234. Springer, Cham, 2016. doi: 10.1007/978-3-319-24609-3_9.

44. R. Jaquet. Investigation of the global second-derivative non-adiabatic contributions: Rovibrational energies of H_2^+, H_2, and prospects for H_3^+ (Part II). *J. Mol. Spectrosc.*, 384:111585, 2022. doi: 10.1016/j.jms.2022.111585.

45. M. Kasha. Characterization of electronic transitions in complex molecules. *Discuss. Faraday Soc.*, 9:14–19, 1950. doi: 10.1039/DF9500900014.

46. J. C. Kromann. Calculate root-mean-square deviation (rmsd) of two molecules using rotation. URL: `https://github.com/charnley/rmsd`, accessed 2024.

47. S. H. Lin and H. Eyring. Study of the Franck–Condon and Herzberg–Teller approximations. *Proc. Nat. Acad. Sci. U.S.A.*, 71(10):3802–3804, 1974. doi: 10.1073/pnas.71.10.3802.

48. H. Lischka, R. Shepard, R. M. Pitzer, I. Shavitt, M. Dallos, T. Müller, P. G. Szalay, M. Seth, G. S. Kedziora, S. Yabushita, et al. High-level multireference methods in the quantum-chemistry program system COLUMBUS: Analytic MR-CISD and MR-AQCC gradients and MR-AQCC-LRT for excited states, GUGA spin–orbit CI and parallel CI density. *Phys. Chem. Chem. Phys.*, 3(5):664–673, 2001. doi: 10.1039/B008063M.

49. S. Maeda, K. Ohno, and K. Morokuma. Updated branching plane for finding conical intersections without coupling derivative vectors. *J. Chem. Theory Comput.*, 6(5):1538–1545, 2010. doi: 10.1021/ct1000268.

50. G. Marconi and P. Salvi. Vibronic activity in the fluorescence and absorption spectrum of pyrene. *Chem. Phys. Lett.*, 123(4):254–260, 1986. doi: 10.1016/0009-2614(86)80067-7.

51. S. Nangia, A. W. Jasper, T. F. Miller III, and D. G. Truhlar. Army ants algorithm for rare event sampling of delocalized nonadiabatic transitions by trajectory surface hopping and the estimation of sampling errors by the bootstrap method. *J. Chem. Phys.*, 120 (8):3586–3597, 2004. doi: 10.1063/1.1641019.

52. S. Nangia, A. W. Jasper, I. Miller, Thomas F., and D. G. Truhlar. Erratum: "Army ants algorithm for rare event sampling of delocalized nonadiabatic transitions by trajectory surface hopping and the estimation of sampling errors by the bootstrap method" [J. Chem. Phys. 120, 3586 (2004)]. *J. Chem. Phys.*, 144(13):139901, 2016. doi: 10.1063/1.4944694.

53. F. Neese, F. Wennmohs, U. Becker, and C. Riplinger. The ORCA quantum chemistry program package. *J. Chem. Phys.*, 152(22):224108, 2020. doi: 10.1063/5.0004608.

54. Y. Niu, Q. Peng, C. Deng, X. Gao, and Z. Shuai. Theory of excited state decays and optical spectra: Application to polyatomic molecules. *J. Phys. Chem. A*, 114(30):7817–7831, 2010. doi: 10.1021/jp101568f.

55. G. Orlandi and W. Siebrand. Mechanisms of vibronic intensity borrowing. *Chem. Phys. Lett.*, 15(4):465–468, 1972. doi: 10.1016/0009-2614(72)80350-6.

56. Q. Ou, G. D. Bellchambers, F. Furche, and J. E. Subotnik. First-order derivative couplings between excited states from adiabatic TDDFT response theory. *J. Chem. Phys.*, 142(6):064114, 2015. doi: 10.1063/1.4906941.

57. M. Parac and S. Grimme. A TDDFT study of the lowest excitation energies of polycyclic aromatic hydrocarbons. *Chem. Phys.*, 292(1):11–21, 2003. doi: 10.1016/S0301-0104(03)00250-7.

58. S. M. Parker, S. Roy, and F. Furche. Unphysical divergences in response theory. *J. Chem. Phys.*, 145(13):134105, 2016. doi: 10.1063/1.4963749.

59. S. M. Parker, D. Rappoport, and F. Furche. Quadratic response properties from TDDFT: Trials and tribulations. *J. Chem. Theory Comput.*, 14(2):807–819, 2018. doi: 10.1021/acs.jctc.7b01008.

60. S. M. Parker, S. Roy, and F. Furche. Multistate hybrid time-dependent density functional theory with surface hopping accurately captures ultrafast thymine photodeactivation. *Phys. Chem. Chem. Phys.*, 21(35):18999–19010, 2019. doi: 10.1039/C9CP03127H.

61. J. P. Perdew, M. Ernzerhof, and K. Burke. Rationale for mixing exact exchange with density functional approximations. *J. Chem. Phys.*, 105(22):9982–9985, 1996. doi: 10.1063/1.472933.

62. F. Plasser, G. Granucci, J. Pittner, M. Barbatti, M. Persico, and H. Lischka. Surface hopping dynamics using a locally diabatic formalism: Charge transfer in the ethylene

dimer cation and excited state dynamics in the 2-pyridone dimer. *J. Chem. Phys.*, 137 (22):22A514, 2012. doi: 10.1063/1.4738960.

63. J. R. Platt. Classification of spectra of cata-condensed hydrocarbons. *J. Chem. Phys.*, 17(5):484–495, 1949. doi: 10.1063/1.1747293.

64. D. Rappoport and F. Furche. Property-optimized gaussian basis sets for molecular response calculations. *J. Chem. Phys.*, 133(13):134105, 2010. doi: 10.1063/1.3484283.

65. M. K. Roos, S. Reiter, and R. de Vivie-Riedle. Ultrafast relaxation from ^1L_a to ^1L_b in pyrene: a theoretical study. *Chem. Phys.*, 515:586–595, 2018. doi: 10.1016/j.chemphys.2018.08.002.

66. S. Roy, S. Ardo, and F. Furche. 5-methoxyquinoline photobasicity is mediated by water oxidation. *J. Phys. Chem. A*, 123(31):6645–6651, 2019. doi: 10.1021/acs.jpca.9b05341.

67. J. Schirmer. Beyond the random-phase approximation: A new approximation scheme for the polarization propagator. *Phys. Rev. A*, 26(5):2395–2416, 1982. doi: 10.1103/physreva.26.2395.

68. R. Send and F. Furche. First-order nonadiabatic couplings from time-dependent hybrid density functional response theory: Consistent formalism, implementation, and performance. *J. Chem. Phys.*, 132(4):044107, 2010. doi: 10.1063/1.3292571.

69. I. Tamm. Relativistic interaction of elementary particles. In B. M. Bolotovskii, V. Y. Frenkel, and R. Peierls, editors, *Selected Papers*, chapter N.4, pages 157–174. Springer, Berlin Heidelberg, 1 edition, 1991. ISBN 9783-64274-62-8-4. doi: 10.1007/978-3-642-74626-0_12.

70. E. Tapavicza. Generating function approach to single vibronic level fluorescence spectra. *J. Phys. Chem. Lett.*, 10(20):6003–6009, 2019. doi: 10.1021/acs.jpclett.9b02273.

71. E. Tapavicza, A. M. Meyer, and F. Furche. Unravelling the details of vitamin D photosynthesis by non-adiabatic molecular dynamics simulations. *Phys. Chem. Chem. Phys.*, 13(47):20986–20998, 2011. doi: 10.1039/C1CP21292C.

72. E. Tapavicza, G. D. Bellchambers, J. C. Vincent, and F. Furche. Ab initio non-adiabatic molecular dynamics. *Phys. Chem. Chem. Phys.*, 15(42):18336–18348, 2013. doi: 10.1039/C3CP51514A.

73. E. Tapavicza, F. Furche, and D. Sundholm. Importance of vibronic effects in the UV–Vis spectrum of the 7,7,8,8-tetracyanoquinodimethane anion. *J. Chem. Theory Comput.*, 12 (10):5058–5066, 2016. doi: 10.1021/acs.jctc.6b00720.

74. E. Tapavicza, T. Thompson, K. Redd, and D. Kim. Tuning the photoreactivity of *Z*-hexatriene photoswitches by substituents–a non-adiabatic molecular dynamics study. *Phys. Chem. Chem. Phys.*, 20(38):24807–24820, 2018. doi: 10.1039/C8CP05181J.

75. A. M. Tokmachev, M. Boggio-Pasqua, M. J. Bearpark, and M. A. Robb. Photostability via sloped conical intersections: A computational study of the pyrene radical cation. *J. Phys. Chem. A*, 112(43):10881–10886, 2008. doi: 10.1021/jp8044109.

76. A. B. Trofimov and J. Schirmer. An efficient polarization propagator approach to valence electron excitation spectra. *J. Phys. B: At., Mol. Opt. Phys.*, 28(12):2299–2324, 1995. doi: 10.1088/0953-4075/28/12/003.

77. J. C. Tully. Molecular dynamics with electronic transitions. *J. Chem. Phys.*, 93(2): 1061–1071, 1990. doi: 10.1063/1.459170.

78. N. J. Turro, V. Ramamurthy, W. Cherry, and W. Farneth. The effect of wavelength on organic photoreactions in solution. reactions from upper excited states. *Chem. Rev.*, 78 (2):125–145, 1978. doi: 10.1021/cr60312a003.

79. L. Verlet. Computer "experiments" on classical fluids. I. Thermodynamical properties of Lennard–Jones molecules. *Phys. Rev.*, 159(1):98–103, 1967. doi: 10.1103/physrev.159.98.

80. K. Veys and D. Escudero. Anti-Kasha fluorescence in molecular entities: Central role of electron–vibrational coupling. *Acc. Chem. Res.*, 55(18):2698–2707, 2022. doi: 10.1021/acs.accounts.2c00453.

81. J. C. Vincent, M. Muuronen, K. C. Pearce, L. N. Mohanam, E. Tapavicza, and F. Furche. That little extra kick: Nonadiabatic effects in acetaldehyde photodissociation. *J. Phys. Chem. Lett.*, 7(20):4185–4190, 2016. doi: 10.1021/acs.jpclett.6b02037.

82. M. W. Walker, L. Shao, and R. A. Volz. Estimating 3-D location parameters using dual number quaternions. *CVGIP Image Underst.*, 54(3):358–367, 1991. doi: 10.1016/1049-9660(91)90036-OO.

83. Y.-L. Wang and G.-S. Wu. Improving the TDDFT calculation of low-lying excited states for polycyclic aromatic hydrocarbons using the Tamm–Dancoff approximation. *Int. J. Quantum Chem.*, 108(3):430–439, 2008. doi: 10.1002/qua.21510.

84. F. Weigend and R. Ahlrichs. Balanced basis sets of split valence, triple zeta valence and quadruple zeta valence quality for H to Rn: Design and assessment of accuracy. *Phys. Chem. Chem. Phys.*, 7(18):3297–3305, 2005. doi: 10.1039/B508541A.

85. A. White, S. Tretiak, and D. Mozyrsky. Coupled wave-packets for non-adiabatic molecular dynamics: a generalization of gaussian wave-packet dynamics to multiple potential energy surfaces. *Chem. Sci.*, 7(8):4905–4911, 2016. doi: 10.1039/C6SC01319H.

86. T. J. Zuehlsdorff, A. Montoya-Castillo, J. A. Napoli, T. E. Markland, and C. M. Isborn. Optical spectra in the condensed phase: Capturing anharmonic and vibronic features using dynamic and static approaches. *J. Chem. Phys.*, 151(7):074111, 2019. doi: 10.1063/1.5114818.